How to specify super-smooth mirrors: simulation studies on nano-focusing and wavefront preserving X-ray mirrors for next-generation light sources

Xianbo Shi*, Lahsen Assoufid, Ruben Reininger
Advanced Photon Source, Argonne National Laboratory, Argonne, Illinois 60439, USA

ABSTRACT

The advent of high-brilliance synchrotron radiation sources with low emittance and high degree of coherence has urged the development of super-smooth X-ray mirrors, which have sub-nanometer height errors and sub-50-nrad slope errors. To ensure the optical performance and avoid procuring significantly more expensive mirrors than necessary, knowledge of the mirror surface power spectral density (PSD) function is required over a wide spatial frequency range. In addition, a better understanding of the diffraction effects of different spatial frequencies is required to guide the specification of the mirror in the beamline design phase. In this work, two typical x-ray beam focusing conditions for the proposed APS upgrade are studied: the diffraction limited focusing and the demagnification dominated focusing. The effects of surface errors are studied using both the method described by Church and Takacs[1] and numerical simulations with *HYBRID*[2]. Using this information, we show how the mirror specification depends on the mirror PSD.

Keywords: X-ray mirrors, specification, X-ray optics simulation, power spectral density, figure errors, metrology

1. INTRODUCTION

The existing[3–6] and planned[7,8] x ray free-electron laser sources as well as the new synchrotron radiation sources based on multiple bend achromat lattices being commissioned[9], constructed[10] and in the design phase[11–14] require optical elements with stringent requirements capable of taking full advantage of the very small machine emittance.

The specification of optics for the third (and previous) synchrotron radiation facilities was, in most cases, based on two parameters: the RMS slope errors and RMS roughness. The use of these specifications was based on the work of Church and Takacs[1] who, as detailed in section 2, showed that the decrease on the on-axis intensity could be separated on two contributions: a photon energy independent contribution related to the slope errors, and an energy dependent related to the surface roughness.

Pardini et al.[15] have recently shown that for optics to be used at FEL facilities the stringent slope errors obtained from geometric arguments do not provide a significant improvement over slightly larger slope errors. Evidently, optics with the stringent slope errors are harder to manufacture and therefore more expensive. Yashchuk et al.[16] investigated the applicability of using the slope error PSD to predict a mirror performance on a FEL beamline. They concluded that slope error is not sufficient to uniquely determine the expected performance.

We are presently considering the requirement of the optics for the beamlines that will take full advantage of the over two orders of magnitude smaller emittance to be provided by the upgrade of the Advanced Photon Source[11]. Furthermore, we are considering how this optics should be properly specified such as not to increase its cost without adding performance. In this paper, we use the *HYBRID* code[2,17,18] to study the effect of single spatial frequencies on the expected performance of mirrors in two cases: diffraction limited and demagnification dominated focusing. Subsequently, the expected performance of these two types of mirrors is quantified in terms of the PSD of the residual heights.

*xshi@aps.anl.gov; phone 1 630 252-9676; fax 1 630 252-9303

AOMATT 2016: Subnanometer Accuracy Measurement for Synchrotron Optics and X-Ray Optics, edited by Shinan Qian, Mourad Idir, Daniele Cocco, Tiqiao Xiao, Kazuto Yamauchi, Proc. of SPIE Vol. 9687, 968703

2. METHODS AND CASE DESCRIPTION

2.1 The Strehl ratio approach

In the smooth-surface limit, the residual height error $h(x)$ of a grazing-incidence mirror can be represented as a Gaussian random distribution. According to Church and Takacs[1], the most important attribution that describe the image quality is the on-axis Strehl ratio, which is the ratio of the on-axis intensity, $I(0)$, in the presence of figure errors to that of the ideal optics $I_0(0)$, or

$$\frac{I(0)}{I_0(0)} = 1 - \left(\frac{4\pi}{\lambda}\sin\theta\right)^2 \sigma_{eff}^2 , \tag{1}$$

where λ is the x-ray wavelength, θ is the grazing incident angle, and

$$\sigma_{eff}^2 = \int_0^\infty PSD(f)\left[1 - \exp\left(-W^2 f^2\right)\right] df . \tag{2}$$

The $PSD(f)$ is the power spectral density of the figure height error, $f = 1/x$ is the spatial frequency, and the critical length W is defined as

$$W = \frac{\sqrt{2}\lambda}{\Theta \sin\theta} , \tag{3}$$

where Θ is the angular size of the image. Physically, figure errors with spatial wavelength smaller than W diffracts the beam out of the angular size Θ of the image. In the case of diffraction-limited optics, W is larger than the mirror length L. On the other hand, most of the mirrors used at the second- and third-generation synchrotron light sources are still limited by the geometrically source demagnification, and therefore W is much less than L. As a result, Eq. (1) is normally written in its approximate form[1]

$$\frac{I(0)}{I_0(0)} \approx 1 - \frac{8}{\Theta^2}\mu^2 - \left(\frac{4\pi}{\lambda}\sin\theta\right)^2 \sigma^2 , \tag{4}$$

where μ and σ are the RMS residual slope error and height error (roughness) of the surface given by

$$\mu^2 = (2\pi)^2 \int_{1/L}^{1/W} PSD(f) f^2 df , \tag{5}$$

and

$$\sigma^2 = \int_{1/W}^{1/\lambda} PSD(f) df , \tag{6}$$

respectively. The separation of the two terms corresponds to the physical division of the "figure" and "finish" errors. As super-smooth mirrors are required for the diffraction-limited light sources, this separation becomes less straightforward. A simple μ or σ value is not adequate for specifying such mirrors. Instead, the full knowledge of the $PSD(f)$ is needed.

2.2 System performance based on numerical simulation

The specification of mirrors must be based on the expected system performance. Numerical simulations of the beam profiles are thus essential for the beamline design and optics specification. Ray-tracing codes based on geometrical optics (e.g., *SHADOW*[19,20], *RAY*[21] and McXtrace[22]) have been widely used for x-ray optics simulations. Ray-tracing codes treat the low spatial frequency ($1/L<f<1/W$) slope errors correctly, but not applicable to high spatial frequency ($1/W<f<1/\lambda$) height errors. Since the super-smooth mirrors in the scope of this paper have W values close to or even larger than L, geometrical ray-tracing is not suitable. Instead, wave optics propagation codes (e.g., *SRW*[23,24] and

PHASE[25,26]), or codes that combine ray-tracing and wavefront propagation (xrt[27] and *HYBRID*[2,17,18]) can be used. The *HYBRID* code is used for simulating all the beam profiles in this work.

The undulator source used in the simulation is approximated by a Gaussian distribution with RMS size and divergence given by[28]

$$\Sigma_s = \left(\sigma_e^2 + \frac{\lambda L_u}{2\pi^2} \right)^{1/2}, \tag{7}$$

and

$$\Sigma'_s = \left(\sigma'^2_e + \frac{\lambda}{2L_u} \right)^{1/2}, \tag{8}$$

where L_u is the undulator length, and σ_e and σ'_e are the RMS size and divergence of the electron beam, respectively.

The figure-error profile $\Delta h(l)$ of the grazing-incidence mirror is constructed by a sum of cosine components $\Delta h_n(l)$ with frequencies that are multiples of $1/L$, or

$$\Delta h(l) = \sum_n \Delta h_n(l) = \sum_n b_0 n^{s_0/2} \cos\left(\frac{2\pi n}{L} l + \psi_n \right), \tag{9}$$

where b_0 is an adjustable parameter, s_0 is the slope of the linear fitting of $\log[PSD(f)]$ as a function of $\log(f)$, and ψ_n is a random phase shift. DABAM[29], an open-source database of x-ray mirrors metrology, contains metrology data obtained from different facilities. By analyzing all the available metrology data (26 so far) on DABAM, we obtain that s_0 varies in the range of -1.0 to -5.5.

Once the beam profile is simulated using *HYBRID*, the focus quality is evaluated by means of (a) the on-axis Strehl factor extracted as the ratio of the peak intensity with the non-ideal mirror to that with the ideal mirror, and (b) the relative RMS beam size defined as the ratio between the RMS beam size with the non-ideal mirror to that with the ideal mirror. The RMS beam size of an image profile is defined as the RMS size within the spatial range containing 90% of the beam intensity

2.3 Focusing mirrors for the APS upgrade

The proposed APS upgrade with the Multi-Bend Achromat (MBA) lattice will increase the brightness of the emitted radiation by more than two orders of magnitude. The low source emittance implies smaller beam size and divergence and therefore, more stringent optics quality requirements. Using the MBA lattice design parameters and Eqs. (7) and (8), the source sizes and divergences at 10 keV of a L_u = 4.8 m long undulator are calculated to be Σ_v = 6.8 μm and Σ'_v = 4.0 μrad in the vertical direction, and Σ_h = 22.5 μm and Σ'_h = 4.8 μrad in the horizontal direction. Here, two cases are considered: (i) a diffraction-limited focusing, namely: a 70 mm long mirror located at 70 m from the source focusing the vertical beam with a 70 mm focal distance (demagnification of 1:1000), and (ii) a demagnification dominated focusing case: a 400 mm long mirror located at 70 m from the source focusing the horizontal beam with a 700 mm focal distance (demagnification of 1:100). The angular sizes of the focused beam profile are obtained from the *HYBRID* simulation with ideal mirrors. The critical lengths are calculated using Eq. (3). The parameters for the two focusing cases are summarized in Table 1.

In the diffraction limited focusing case, W is larger than L, which suggests that the mirror should be described solely in terms of height errors. This condition is commonly found for mirrors at XFEL facilites[15,16]. For the APS upgrade, the diffraction limited mirror accepts about 30% of the vertical fan. The 400 mm mirror is able to accept nearly the full beam. Therefore, the conclusions obtained for the demagnification dominated focusing mirror are also applicable to general deflection mirrors and high heat load mirrors for the APS upgrade that accept the full beam. The critical length in this case is W = 79 mm which is one fifth the mirror length. Since the justification of using Eqs (5) and (6) is borderline, we will use instead, Eqs (1) and (2) with the full PSD function.

Table 1. System parameters used for the two cases.

	Diffraction limited focusing	Demagnification dominated focusing
Source size, Σ_s (μm)	6.8	22.5
Source divergence, Σ'_s (μrad)	4.0	4.8
Source-to-mirror distance, f_1 (m)	70	70
Mirror-to-image distance, f_2 (mm)	70	700
Mirror length, L (mm)	70	400
Grazing angle, θ (mrad)	3	3
Image angular size, Θ (μrad)	0.49	0.74
Critical length, W (mm)	118	79
Mirror acceptance	30%	93%

3. SINGLE SPATIAL FREQUENCY STUDIES

The frequency dependence of the slope and height errors is studied by examining the focusing performance under the influence of a surface error with a single spatial frequency. For a particular spatial frequency (n/L), cosine surface error functions $\Delta h_n(l)$ are generated based on

$$\Delta h_n(l) = A\cos\left(\frac{2\pi n}{L}l + \psi_n\right). \tag{10}$$

By adjusting the parameter A, we construct surface error profiles with different RMS height errors and RMS slope errors following

$$\sigma = \frac{A}{\sqrt{2}}, \quad \mu = \frac{\sqrt{2}A\pi n}{L}. \tag{11}$$

As an example, Fig. 1(a) shows the simulated image profiles using *HYBRID* with a mirror figure error having a single spatial frequency [n = 5 in Eq. (9)] for different RMS height errors (σ). From these image profiles, the Strehl ratios are extracted and plotted as a function of σ as presented in Fig. 1(b). Fig. 1(b) was then used to obtain the RMS height error for which the Strehl ratio was arbitrarily chosen as 0.9.

The same analysis was performed for different n values ($1 \le n \le 100$), obtaining the RMS height error for which the Strehl ratio is 0.9. Figs. 2(a) and 2(b) presents these results for the focusing cases studied here.

For the diffraction limited focusing case [cf. Fig. 2(a)], the maximum RMS height error to ensure a Strehl ratio of 0.9 is very close to 1nm for all spatial frequencies larger than 1. Frequency n = 1 strongly depends on the choice of the phase shift ψ_n in Eq. (9). This means that for surface errors with a combination of frequencies the RMS height error is an adequate criterion for specifying a diffraction limited mirror. It should be pointed out that this fact is consistent with the result of Eq. (3), W = 118 mm which is larger than the mirror length. On the other hand as demonstrated in Fig. 2(a), the maximum RMS slope error varies dramatically with spatial frequencies. Therefore, one cannot use a single slope error value to specify a real mirror. If a Strehl ratio of 0.81 is used as the criterion, the maximum RMS height error is obtained to be 1.4 nm for all frequencies. This is consistent with the Maréchal criterion of $\sigma_M \approx 1.5$ nm given by[30]

$$\sigma_M = \frac{\lambda}{28\sin\theta}. \tag{12}$$

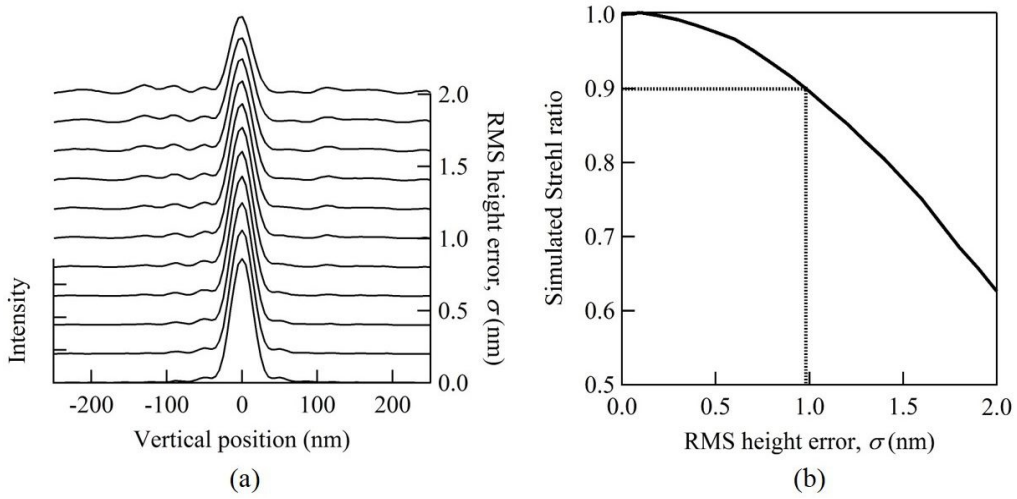

Figure 1. (a) Simulated image profiles for different RMS height errors with a single spatial frequency [n = 5 in Eq. (9)]. The graces are staggered vertically as given by the right axis. (b) The extracted Strehl ratio from profiles in (a) as a function of the RMS height error. The dotted line indicates where the Strehl ratio equals to 0.9.

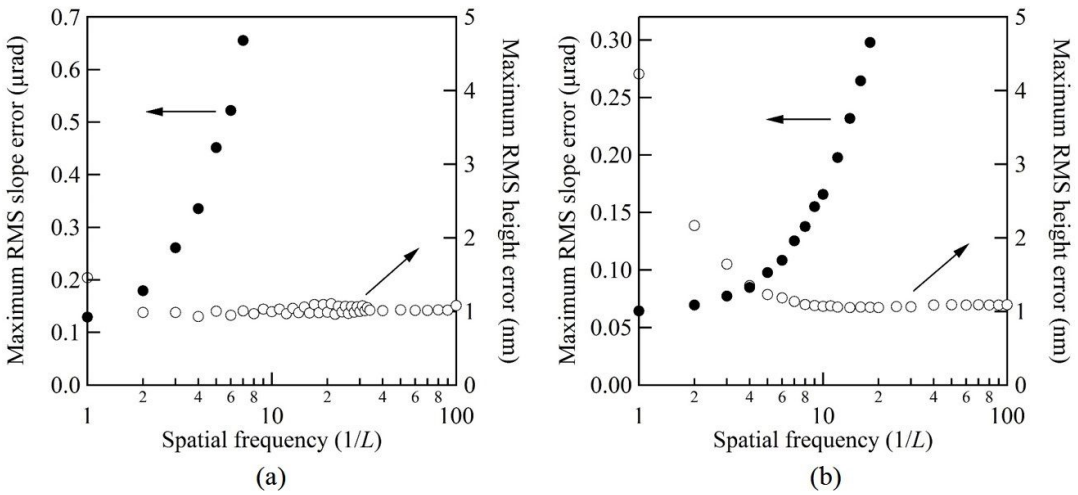

Figure 2. Extracted maximum RMS slope error (solid markers) and maximum RMS height error (open markers) as a function of the spatial frequency n for (a) the diffraction limited focusing case and (b) the demagnification dominated focusing case.

For the demagnification dominated focusing case [cf. Fig. 2(b)], neither the RMS slope error nor the RMS height error can be solely used to describe the mirror. In this case, the maximum RMS slope error increases moderately (from 0.06 to 0.08 μrad) up to a frequency of 5/L, while the maximum RMS height error tends to become constant (~1 nm) above that frequency. This boundary (L/5 = 80 mm) is consistent with the W value obtained from Eq. (3) (cf. Table 1). However, it is difficult and not realistic to set a hard boundary between the two types of contributions. Of course, one can always specify the mirror with the most stringent requirement which is to keep the RMS slope error below 0.07 μrad and the RMS height error below 1 nm for the entire frequency range. The over specification of the mirror may result in difficulties finding manufacturers and increasing the cost and the delivery time.

4. MIRROR PSD STUDIES

In this section we study the effects of PSDs with different s_0 values within the range of -1.5 to -3.5. Surface profiles with different RMS slope errors and RMS height errors are generated based on Eq. (9) by adjusting the parameter b_0. The

HYBRID method provides an efficient way of simulating mirror performance taking into account the partial coherence of the source, which is useful for the beamline design for next-generation light sources.

4.1 Diffraction limited focusing simulation

Fig. 3(a) shows three surface error profiles with the same RMS height error (σ = 1 nm) generated using Eq. (9). The corresponding RMS slope errors are calculated to be μ = 1.47, 0.33 and 0.13 μrad, for s_0 = -1.5, -2.5 and -3.5, respectively. The simulated focusing profiles with the three mirror errors are presented in Fig. 3(b) together with the one using the ideal elliptical cylinder mirror. Similarly, three surface error profiles with the same RMS slope error (μ = 0.3 μrad) are created and shown in Fig. 4(a). The corresponding RMS height errors are σ = 0.20, 0.91 and 2.29 nm. The simulated focusing profiles are shown in Fig. 4(b). The image qualities are represented in terms of the on-axis Strehl ratio and the relative RMS beam size (see Section 2.2 for details). Note that the profiles with surface errors all have slightly shifted central peaks, which is due to the low-frequency error term [ψ_1 in Eq. (9)]. The simulation results are summarized in Table 2.

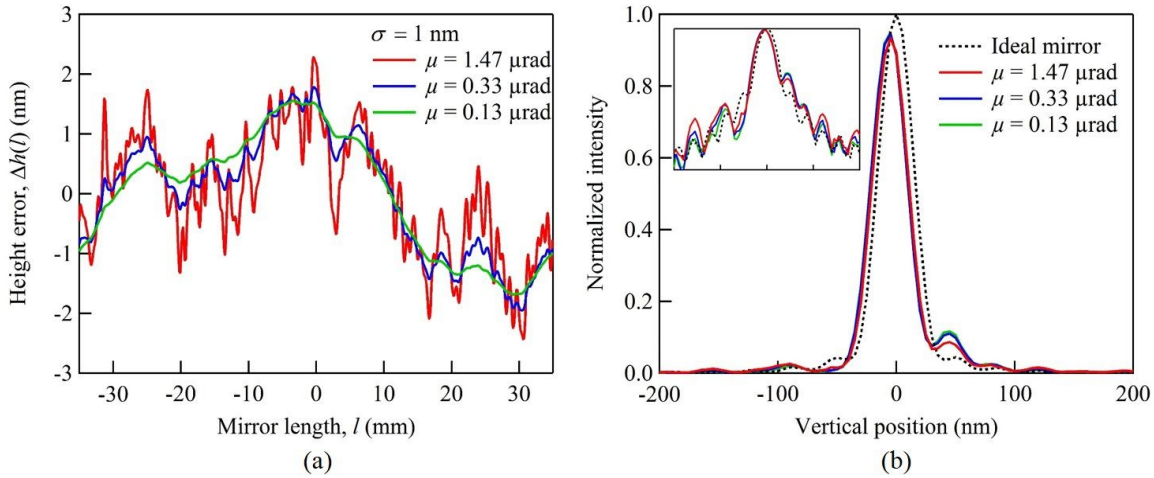

Figure 3. (a) The three surface error profiles generated using Eq. (9), all with σ = 1.0 nm, and μ = 1.47, 0.33 and 0.13 μrad, respectively. (b) The beam intensity profiles (colored solid lines) simulated with surface errors in (a) and the ideal elliptical cylinder mirror (dotted black line). (Insert) The same profiles in a log scale shows the side peaks.

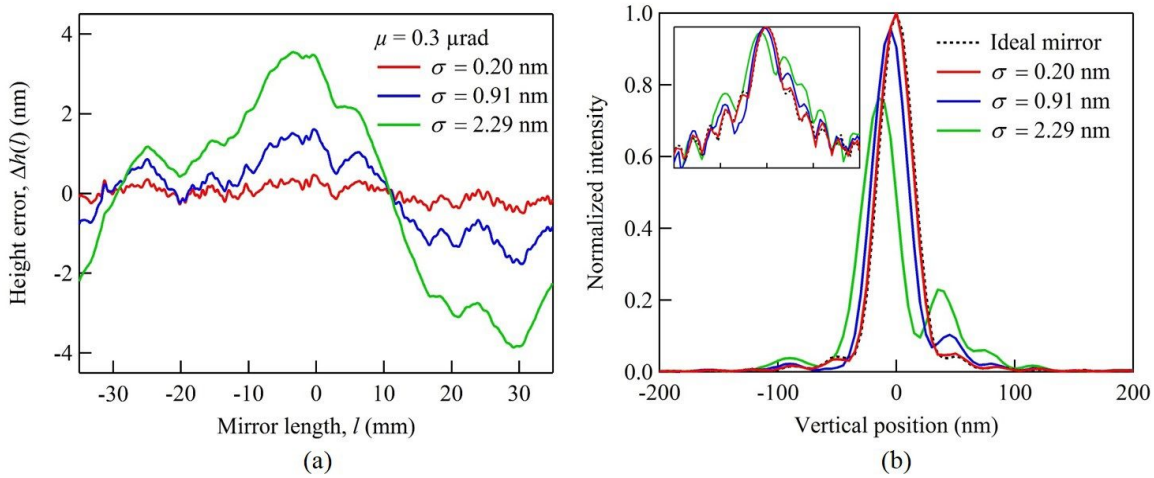

Figure 4. (a) The three surface error profiles generated using Eq. (9), all with μ = 0.30 μrad, and σ = 0.20, 0.91 and 2.29 nm, respectively. (b) The beam intensity profiles (colored solid lines) simulated with surface errors in (a) and the ideal elliptical cylinder mirror (dotted black line). (Insert) The same profiles in a log scale shows the side peaks.

Table 2. Simulation results for the diffraction limited focusing case.

s_0	σ (nm)	μ (μrad)	Strehl ratio Eqs. (1)(2)	Strehl ratio from simulation	Relative RMS beam size
-1.5	1.0	1.47	0.91	0.93	1.17
-2.5	1.0	0.33	0.91	0.95	1.21
-3.5	1.0	0.13	0.91	0.95	1.22
-1.5	0.20	0.30	1.00	1.00	1.00
-2.5	0.91	0.30	0.93	0.96	1.19
-3.5	2.29	0.30	0.54	0.76	1.91

With the same RMS height error of 1 nm, the slope error can vary over a large range depending on the s_0 value [cf. Fig. 3(a)]. However, the image profiles show very similar properties (cf. Fig. 3(b) and Table. 2). Since Eq. (5) vanishes for the diffraction limited mirror ($W>L$), the same height error implies the same total intensity scattered out of the central peak. The use of different PSD(f) with different s_0 values only changes the distribution of the scattered intensity. For instance, the mirror with the largest slope error (red curve in Fig. 3(a) with s_0 = -1.5) has the largest high-frequency contributions and the lowest low-frequency contributions, therefore, the image profile [red curve in Fig. 3(b)] shows the lowest intensity of the side peak to the right side of the central peak as comparison with the other two mirrors. More intensities are scattered further from the central peak by the high-frequency components of the height error. As shown in Table 2, the extracted on-axis Strehl ratios are very close for all three mirrors and agrees well with the values calculated using Eqs. (1) and (2). The relative RMS beam size also shows the same trend.

Fig. 4 shows that the RMS slope error is not a good criterion for a diffraction limited mirror specification. With the same μ but different σ values, the image profiles vary significantly taking significant intensity from the main peak. The comparisons show in Table 2 between the Strehl ratio obtained from Eqs. 1 and 2 are in reasonable agreement with the values obtained from the full simulation.

4.2 Demagnification dominated focusing simulation

In this case, neither the single μ value nor the single σ value can be used to solely describe the mirror. Fig. 5 presents the simulation results of three surface error profiles with the same σ = 3.0 nm, but different μ values (0.75, 0.17 and 0.07 μrad). Fig. 6 shows the results of three mirrors with the same μ = 0.17 μrad, but different σ values (0.7, 3.0 and 7.4 nm). The simulated image profiles, shown in Fig. 5(b) and 6(b), demonstrate similar results, namely that the on axis intensity decreases and the image gets broader. The extracted Strehl ratio and relative RMS beam size are summarized in Table 3. In order to appropriately specify this mirror, the PSD(f) over the full spatial frequency has to be considered.

One possibility is to use the on-axis Strehl ratio calculated from Eqs. (1) and (2) as the criterion for the mirror specification. To validate the correctness of such approach, five surface error profiles are generated with completely different PSD (f) [cf. Fig. 7(a)] and shown in Fig. 7(b). The magnitude of all the PSD(f) are scaled so that the Strehl ratios calculated from Eqs. (1) and (2) equal to 0.9. The RMS height and slope errors of these profiles are σ = 1.7, 2.3, 3.0, 3.6 and 4.3 nm, and μ = 0.43, 0.27, 0.17, 0.12 and 0.10 μrad, respectively. The simulated image profiles [cf. Fig. 7(c)] show similar sizes and intensities. The extracted Strehl ratios and relative RMS beam sizes shown in Table 3 are almost the same for all five error profiles. The simulated Strehl ratios agree well with the ones calculated using Eqs. (1) and (2). In terms of optical performance, the five surface error profiles are considered to be equivalent despite the difference in their statistical properties. The use of on-axis Strehl ratio based on PSD(f) provides fairly accurate estimation of the optics quality therefore, it is very useful to obtain the PSD(f) data of different manufacturing techniques and metrology tools from different manufacturers, for instance the DABAM database[29].

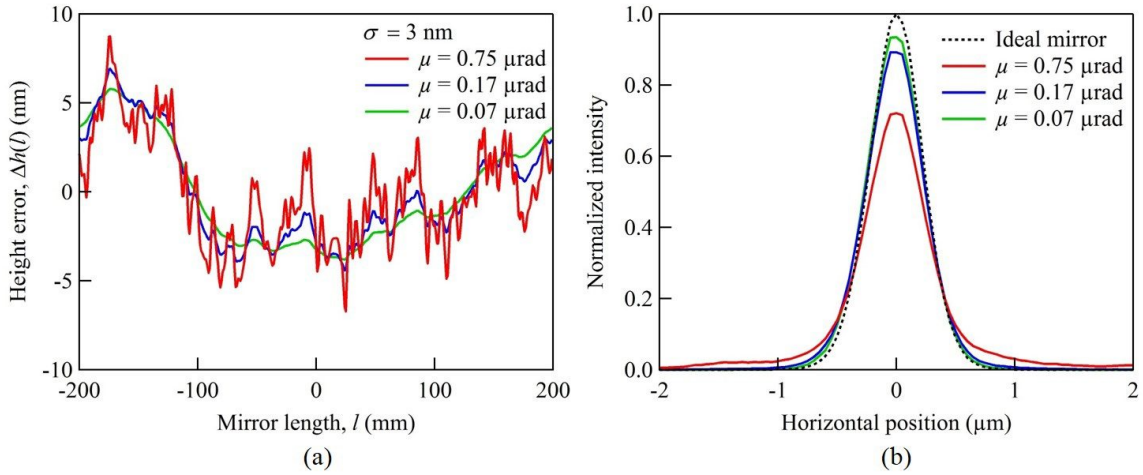

Figure 5. (a) The three surface error profiles generated using Eq. (9), all with σ = 3.0 nm, and μ = 0.75, 0.17 and 0.07 μrad, respectively. (b) The beam intensity profiles (colored solid lines) simulated with surface errors in (a) and the ideal elliptical cylinder mirror (dotted black line).

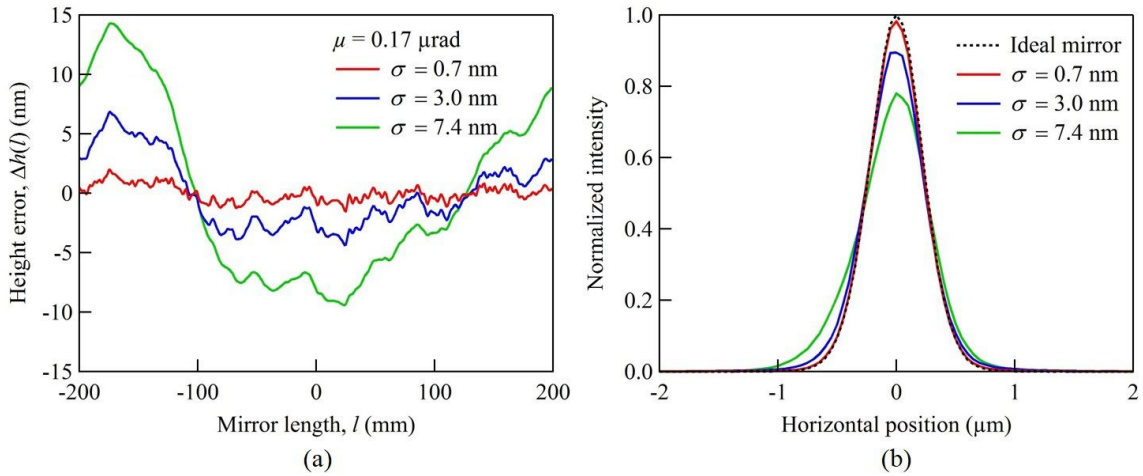

Figure 6. (a) The three surface error profiles generated using Eq. (9), all with μ = 0.17 μrad, and σ = 0.7, 3.0 and 7.4 nm, respectively. (b) The beam intensity profiles (colored solid lines) simulated with surface errors in (a) and the ideal elliptical cylinder mirror (dotted black line).

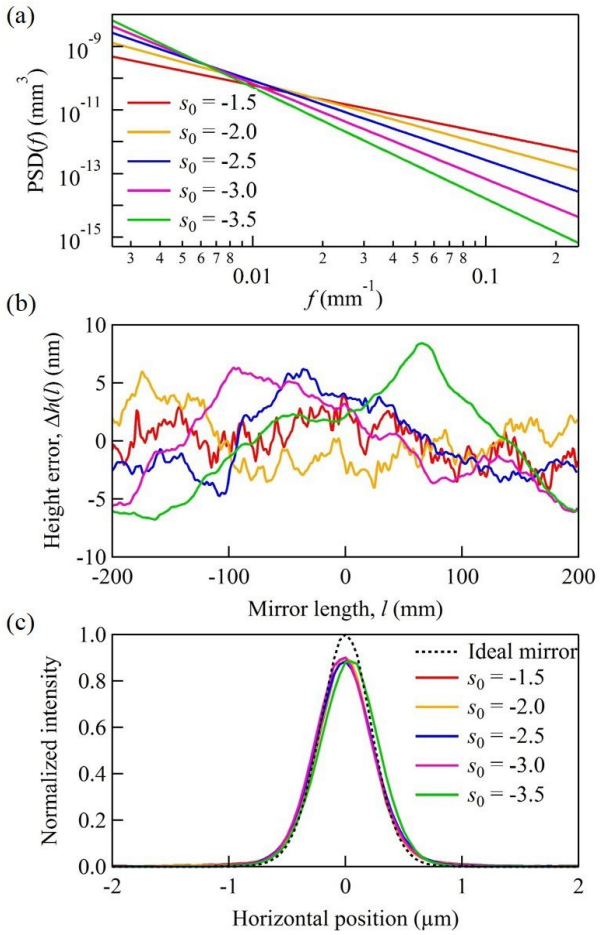

Figure 7. (a) PSD(f) with s_0 = -1.5, -2.0, -2.5, -3.0 and -3.5, respectively. (b) The five surface error profiles generated using Eq. (9) with the PSD from (a). The RMS height errors are σ = 1.7, 2.3, 3.0, 3.6 and 4.3 nm, and the RMS slope errors are μ = 0.43, 0.27, 0.17, 0.12 and 0.10 μrad, respectively. (c) The beam intensity profiles (colored solid lines) simulated with surface errors in (b) and the ideal elliptical cylinder mirror (dotted black line).

Table 3. Simulation results for the demagnification dominated focusing case.

s_0	σ (nm)	μ (μrad)	Strehl ratio Eqs. (1)(2)	Strehl ratio from simulation	Relative RMS beam size
-1.5	3.0	0.75	0.70	0.72	1.60
-2.5	3.0	0.17	0.91	0.89	1.11
-3.5	3.0	0.07	0.95	0.93	1.02
-1.5	0.7	0.17	0.98	0.98	1.00
-2.5	3.0	0.17	0.91	0.89	1.11
-3.5	7.4	0.17	0.69	0.78	1.33
-1.5	1.7	0.43	0.90	0.90	1.09
-2.0	2.3	0.27	0.90	0.90	1.10
-2.5	3.0	0.17	0.90	0.89	1.12
-3.0	3.6	0.12	0.90	0.90	1.11
-3.5	4.3	0.10	0.90	0.88	1.12

5. CONCLUSIONS

Effects of surface errors have been studied by both the analytical approach and numerical simulation. The image quality can be well represented by the on-axis Strehl ratio once the height error PSD is known. In all cases described in this paper, the Strehl ratios extracted from the *HYBRID* simulation agree closely with the values obtained from the classical diffraction theory. The appropriate simulation can provide additional information including the image profile which is important for designing certain imaging systems.

The specification of mirror quality is case dependent. For diffraction limited focusing mirrors, the RMS height error is an adequate measure of the surface quality. The Maréchal criterion[30] corresponding to the Strehl ratio of 0.81 is widely used to specify such mirrors. With the assistance of numerical simulation, the designer can better specify the height error requirements based on different Strehl ratio criteria.

The demagnification dominated focusing mirrors designed for next-generation light sources cannot be described solely by a RMS height or RMS slope error value. The boundary that separates the contributions from slope errors and surface roughness lies in the low spatial frequency range, normally a few multiples of $1/L$. The specification of such mirrors is not straightforward and further studies are still needed. For a figure error profile with a known PSD, the system performance can be characterized by the Strehl ratio and detailed numerical simulation. However, mirror figure errors based on different PSDs can also provide similar image qualities. It is therefore difficult to specify a mirror by requesting a single specific PSD. The DABAM database[29] provides a bank of metrology data of real mirrors measured at different facilities. The database can help the designers specify mirrors through analyzing surface error data that are close to the planned mirrors. It will be useful to further expand the database to include more mirrors and to involve the manufactures. Studies on the correlation of the mirror fabrication process and the height error PSD will be the next step.

ACKNOWLEDGMENTS

This work was supported by the US Department of Energy, Office of Science, Office of Basic Energy Sciences, under Contract No. DE-AC02-06CH11357.

REFERENCES

[1] Church, E. L. "Specification of glancing- and normal-incidence x-ray mirrors," Opt. Eng. 34, 353 (1995).
[2] Shi, X., Reininger, R., Sanchez Del Rio, M. & Assoufid, L. "A hybrid method for X-ray optics simulation: combining geometric ray-tracing and wavefront propagation," J. Synchrotron Radiat. 21, 669–78 (2014).
[3] Allaria, E. et al. "The FERMI@Elettra free-electron-laser source for coherent x-ray physics: Photon properties, beam transport system and applications," New J. Phys. 12, 1–27 (2010).
[4] Ackermann, W. et al. "Operation of a free-electron laser from the extreme ultraviolet to the water window," Nat. Photonics 1, 336–342 (2007).
[5] Emma, P. et al. "First lasing and operation of an ångstrom-wavelength free-electron laser," Nat. Photonics 4, 641–647 (2010).
[6] Ishikawa, T. et al. "A compact X-ray free-electron laser emitting in the sub-ångström region," Nat. Photonics 6, 540–544 (2012).
[7] XFEL. at <http://www.xfel.eu/>
[8] SwissFEL. at <https://www.psi.ch/swissfel/>
[9] Tavares, P. F., Leemann, S. C., Sjöström, M. & Andersson, A. "The MAX IV storage ring project," J. Synchrotron Radiat. 21, 862–77 (2014).
[10] Sirius. at <http://lnls.cnpem.br/sirius-new-brazilian-synchrotron-light-source>
[11] APS upgrade. at <https://www1.aps.anl.gov/aps-upgrade>
[12] ESRF upgrade. at <http://www.esrf.eu/ebs>
[13] Tanaka, H. "Current status of the SPring-8 upgrade project," Synchrotron Radiat. News 27, 23–26 (2014).
[14] Tarawneh, H. et al. "ALS-II, a Potential Soft X-ray, Diffraction Limited Upgrade of the Advanced Light Source," J. Phys. Conf. Ser. 493, 012020 (2014).
[15] Pardini, T., Cocco, D. & Hau-Riege, S. P. "Effect of slope errors on the performance of mirrors for x-ray free

electron laser applications," Opt. Express 23, 31889 (2015).
[16] Yashchuk, V. V., Samoylova, L. V. & Kozhevnikov, I. V. "Specification of x-ray mirrors in terms of system performance: new twist to an old plot," Opt. Eng. 54, 025108 (2015).
[17] Shi, X., Reininger, R., Sanchez del Rio, M., Qian, J. & Assoufid, L. "X-ray optics simulation and beamline design using a hybrid method: diffraction-limited focusing mirrors," Proc. SPIE 9209, 920909 (2014).
[18] Shi, X., Sanchez del Rio, M. & Reininger, R. "A new SHADOW update: integrating diffraction effects into ray-tracing," Proc. SPIE 9209, 920911 (2014).
[19] Cerrina, F. "Ray tracing of recent VUV monochromator designs," Proc. SPIE 503, 68–77 (1984).
[20] Sanchez del Rio, M., Canestrari, N., Jiang, F. & Cerrina, F. "SHADOW3: a new version of the synchrotron X-ray optics modelling package," J. Synchrotron Radiat. 18, 708–16 (2011).
[21] Schäfers, F. [Modern developments in X-ray and neutron optics], Springer-Verlag Berlin Heidelberg, 9–41 (2008).
[22] Bergbäck Knudsen, E. et al. "McXtrace: A Monte Carlo software package for simulating X-ray optics, beamlines and experiments," J. Appl. Crystallogr. 46, 679–696 (2013).
[23] Chubar, O. & Elleaume, P. "Accurate and efficient computation of synchrotron radiation in the near field region," Proc. EPAC98 Conf. 1177–1179 (1998).
[24] Canestrari, N., Chubar, O. & Reininger, R. "Partially coherent X-ray wavefront propagation simulations including grazing-incidence focusing optics," J. Synchrotron Radiat. 21, 1110–1121 (2014).
[25] Bahrdt, J. "Wave-front propagation: design code for synchrotron radiation beam lines," Appl. Opt. 36, 4367 (1997).
[26] Bahrdt, J. & Flechsig, U. "PHASE: a universal software package for the propagation of timedependent coherent light pulses along grazing incidence optics," Proc. SPIE 8141, 81410E1–10 (2011).
[27] Klementiev, K. & Chernikov, R. "Powerful scriptable ray tracing package xrt," Proc. SPIE 9209, 92090A (2014).
[28] Elleaume, P. [Undulators, wigglers their Applications], Taylor and Francis, New York, 69–107 (2003).
[29] Sanchez, M. et al. "DABAM : an open-source database of x-ray mirrors metrology," J. Synchrotron Rad. (2016).
[30] Maréchal, A. "Study of the combined effects of diffraction and geometrical aberrations on the image of a luminous point," Rev. Opt. Theor. Instrum. 26, 257–277 (1947).